Available online at www.sciencedirect.com

ScienceDirect

journal homepage: www.elsevier.com/locate/he

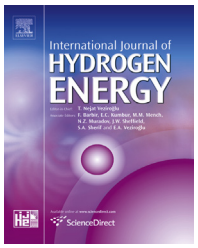

Carbon supported lithium hydride nanoparticles: Impact of preparation conditions on particle size and hydrogen sorption

*Peter L. Bramwell, Peter Ngene, Petra E. de Jongh**

Debye Institute for Nanomaterials Science, Inorganic Chemistry and Catalysis, Utrecht University, Universiteitsweg 99, 3583CG, The Netherlands

ARTICLE INFO

Article history:
Received 26 August 2016
Received in revised form
6 October 2016
Accepted 9 October 2016
Available online 30 October 2016

Keywords:
Hydrogen storage
Lithium hydride
Nanoconfinement
Light metal hydrides

ABSTRACT

Nanosizing of light metal hydrides has yielded significant improvements to their hydrogen storage properties. We explored for the first time a procedure for preparing supported LiH nanoparticles. Impregnation of a carbon framework with a butyllithium solution, followed by reaction with gaseous hydrogen yielded LiH particles ranging in size from 2 nm to the micrometer scale. Reducing the reaction temperature from 300 °C to 100 °C, as well as the use of a t-butyllithium precursor instead of an n-butyllithium precursor, gave significant improvements on the degree of confinement of the LiH particles. The particle size of the LiH has a significant impact on the hydrogen release profile, 11 nm crystallites begin to release hydrogen as low as 100 °C under argon flow, a reduction of roughly 400 °C on the macrocrystalline system. The hydrogen release is reversible, with hydrogen uptake after desorption as high as 7.0 wt% w.r.t. LiH (0.8 wt% w.r.t the sample) under 0.1 bar of hydrogen at 200 °C and full uptake takes place within 5 min at 26 bar. This new preparation procedure for supported light metal hydrides is particularly relevant for the field of hydrogen storage.

Introduction

Light metal hydrides have been investigated for a range of applications including hydrogen storage [1–3] (due to their high gravimetric hydrogen densities) and batteries (in electrodes and solid state electrolytes) [4]. Ideal properties for metal hydrides for the solid state storage of hydrogen for vehicular application are high gravimetric and volumetric hydrogen densities, low temperatures of hydrogen release and uptake, fast kinetics and reversibility. No material has so far been found to possess each of these characteristics but light metal hydrides have displayed the most promise, where modification of the material is hoped to improve their hydrogen sorption characteristics such that they could be viable for application [5–7].

MgH_2 [8–10] and NaH [11] are prominent examples of light metal hydrides investigated for hydrogen storage as they can store 7.6 wt% and 4.2 wt% of hydrogen respectively. A similar, somewhat overlooked, hydride with great promise is lithium hydride, LiH, which contains 12.6 wt% of hydrogen [9,12]. The main reason LiH has not been as extensively studied as other hydrides is that it only releases hydrogen at temperatures above 500 °C, but this might be improved through a number of

* *Corresponding author.*
E-mail address: p.e.dejongh@uu.nl (P.E. de Jongh).
http://dx.doi.org/10.1016/j.ijhydene.2016.10.062

methods. For instance, in general reducing the particle and crystallite size of metal hydrides improves the kinetics of sorption due to shorter diffusion distances of hydrogen while also demonstrating lower temperature of release and enhanced reversibility [13,14]. Additionally, interaction between carbon and Li-based hydrides gives a reduction in hydrogen release temperature due to the reversible intercalation of Li between the graphene sheets promoting decomposition of the hydride [15,16].

Many techniques have been studied in the preparation of small crystallites and particles of light metal hydrides such as ball-milling [17,18] and confinement into a porous matrix [19]. For example, vapor deposition of MgH_2 into a carbon xerogel support has been used to produce MgH_2 particles in the 6–20 nm range [20]. The particle size was controlled by tuning the pore size of the carbon support and the smaller particles demonstrated hydrogen release at temperatures 140 °C lower than the macrocrystalline system under argon flow. Melt infiltration has also been a very useful technique in preparation of a number of metal hydride nanocomposites such as $NaAlH_4$/C [21], which demonstrates a 150 °C reduction in hydrogen release temperature compared to the macrocrystalline system.

However, there are few known examples of the preparation of supported LiH nanoparticles [22–24]. This can be attributed to the fact that many of the common preparation techniques cannot be readily applied to LiH. The high temperatures required to melt LiH initiate reaction between LiH and the carbon support, which means melt infiltration and vapor deposition cannot be used in this case [25,26]. There are a number of alternative methods that have been proposed such as electrochemically inserting lithium into graphite and subsequent hydrogenation to produce nanostructured LiH. This nanostructuring reduces the onset temperature of hydrogen release to 200 °C under argon flow and a total hydrogen capacity of 0.96 wt% [27].

Solution based techniques, such as solution impregnation, are widely used methods of producing nanocomposites [28]. A number of parameters can influence particle size such as the conditions under which the particles are formed. For example, in preparation of supported metal particles from aqueous metal salt precursors the drying step is essential as removal of solvent before precipitation of the metal yields migration of the metal particles to the external surface of the support [28]. For this reason low temperature drying is often necessary. In addition, nucleation sites within the pores facilitate the growth of particles in the pore system and so the density of nucleation sites can be critical to the efficiency of confinement of the particles [28]. Thus, the drying step in solution impregnation techniques is crucial to particle size control and a number of experimental parameters can be tuned to this effect.

However, LiH is insoluble in most solvents [29], and it is therefore necessary to use a precursor from which the desired LiH can be formed. In solution impregnation the loading is limited by the solubility of the precursor as more concentrated solutions allow a higher loading. Incipient wetness impregnation, where the amount of solution equivalent to the pore volume of the support is used, ensures that all of the active component is contained to the pores but this produces low loadings. MgH_2 nanoparticles have been successfully prepared on a carbon support by impregnation with a dibutylmagnesium precursor followed by decomposition and reaction with hydrogen at 300 °C [30,31]. The resulting MgH_2/C nanocomposite gave faster hydrogen release kinetics than ball-milled samples and demonstrated 75% reversibility [30].

Herein we present a procedure, which builds on the previously reported method for supporting MgH_2 nanoparticles [30], for the preparation of a new nanocomposite: LiH/C. This is done by solution impregnation and subsequent reaction of a butyllithium precursor followed by drying under vacuum at room temperature. A number of experimental parameters were varied with the goal of reducing the average particle size of the LiH particles. This includes the type of carbon support, the type of butyllithium precursor and the temperature at which the reaction is performed. This newfound understanding of the solution impregnation procedure can be applied to the preparation of other similar compounds.

Experimental

Materials: *n*-butyllithium (*n*-BuLi, 2.5 M in hexanes) and *tert*-butyllithium (*t*-BuLi, 1.7 M in pentane) were obtained from Sigma–Aldrich. Hydrogen gas was obtained from Linde with a purity of 99.999999%. Butyllithium (BuLi) solutions were stored in a nitrogen-filled glovebox (Mbraun Labmaster I30, 1 ppm H_2O, <1 ppm O_2) prior to use.

Carbon supports: Two different supports were used: carbon xerogel (CX18) and high surface area graphite (HSAG). The carbon xerogel support was prepared using the sol–gel resorcinol procedure [32] and is an amorphous carbon support consisting of micron to millimeter-sized particles containing intra-particle pores. CX18 has a volume average pore diameter of 18 nm. HSAG was obtained from TimCal and is a graphitic-type support with a pore size that ranges from 2 to 50 nm in diameter. It comes in a powder form and consists mostly of graphite sheets. All carbon types were dried under argon flow at 600 °C for 12 h and characterized using X-ray diffraction and nitrogen physisorption before use.

Preparation of the nanocomposites: The LiH/C nanocomposites were prepared by filling a Parr 30 cm^3 autoclave with 10 cm^3 of the butyllithium solution in a nitrogen-filled glovebox, and then adding 1 g of carbon support on top, allowing it to sink to the bottom to ensure complete wetting. The autoclave was then sealed, removed from the glovebox, pressurized with 50 bar hydrogen and heated while stirring for 20 h. Afterwards the autoclave was allowed to cool to room temperature before venting the gas and applying vacuum with a cold trap for 2 h to remove the solvent. The final powder product was then stored in an argon-filled glovebox (Mbraun Labmaster dp, 1 ppm H_2O, <1 ppm O_2) before analysis. With the aim of studying the effect of parameters such as support type, precursor type and temperature of decomposition a number of different nanocomposites were prepared, the details of which are recorded in Table 1. The naming convention used in Table 1 is divided into several parts, each divided by an underscore. The first part refers to the support used, the second refers to the butyllithium isomer used (t = 1.7 M tert-butyllithium in pentane, n = 2.5 M n-butyllithium in hexanes) and the third indicates

Table 1 – List of parameters tested in the preparation of LiH/C nanocomposites.

Sample	Support type[a]	Precursor	Decomposition temperature/°C	LiH loading/wt%
CX18_n_300	CX18	*n*-BuLi	300	17
LiH_n_300	–	*n*-BuLi	300	–
CX18_n_300_PM	CX18	*n*-BuLi	300	17
CX18_n_100	CX18	*n*-BuLi	100	17
LiH_n_100	–	*n*-BuLi	100	–
CX18_n_100_PM	CX18	*n*-BuLi	100	17
CX18_t_300	CX18	*tert*-BuLi	300	12
LiH_t_300	–	*tert*-BuLi	300	–
CX18_t_300_PM	CX18	*tert*-BuLi	300	12
CX18_t_100	CX18	*tert*-BuLi	100	12
LiH_t_100	–	*tert*-BuLi	100	–
CX18_t_100_PM	CX18	*tert*-BuLi	100	12
HSAG_n_300	HSAG	*n*-BuLi	300	17
HSAG_n_300_PM	HSAG	*n*-BuLi	300	17
HSAG_t_100	HSAG	*tert*-BuLi	100	12
HSAG_t_100_PM	HSAG	*tert*-BuLi	100	12

[a] HSAG refers to high surface area graphite, CX18 is a carbon xerogel with an average pore diameter of 18 nm.

the temperature used to decompose the butyllithium. For example HSAG_n_300 refers to a nanocomposite prepared on high surface area graphite, using an n-butyllithium precursor decomposed at 300 °C. The reference sample is denoted with 'PM', for example HSAG_n_300_PM refers to the physical mixture reference material for HSAG_n_300.

For each nanocomposite a reference sample was prepared by synthesizing LiH under the same conditions as the relevant nanocomposite. For example, the reference material for HSAG_n_300 and CX18_n_300 was prepared by decomposing 10 cm^3 of n-butyllithium solution (2.5 M in hexanes) at 300 °C to produce macrocrystalline LiH, which was labelled as LiH_n_300. This was then physically mixed with the HSAG support in the same loading as the nanocomposite. TPD measurements were then performed on each of the physical mixtures and the macrocrystalline LiH as a reference for the nanocomposite (see Supporting information Fig. S1.1).

Leaching of the lithium from each sample was performed to demonstrate that the deposition had not invoked irreversible changes to the support. This was done by immersing a sample of the nanocomposite in 1 M HCl solution for 24 h, then washing 4 times with 100 cm^3 of distilled water and drying in an oven at 120 °C overnight before performing nitrogen physisorption measurements.

X-Ray Diffraction (XRD): X-ray Diffraction measurements (performed with a Bruker AXS D8 advance 120 machine, Co-K_α radiation, air-tight sample holder) were used to determine the amount of crystalline LiH and the crystallite size. The degree of crystallinity of the LiH in each nanocomposite was calculated by comparison to the relevant physical mixture. In both the nanocomposite and the physical mixture the ratio of the areas of the LiH peaks (at $2\theta = 44.5°$, 77.0° and 93.0°) to the area of the main carbon peak at $2\theta = 30°$ was calculated. In the determination of the peak areas the amorphous portion of the sample is also taken into account. The crystallinity in each physical mixture was assumed to be 100% and so the LiH:C peak area ratio of the nanocomposite was normalized to that of the physical mixture. For example, in the CX18_n_300 nanocomposite the LiH:C peak area ratio was 0.034, while that of CX18_n_300_PM was 0.073 and so the crystallinity of CX18_n_300 was determined to be 52%. It can therefore be assumed that any differences in crystallinity between the physical mixture and the nanocomposite are due to confinement within the pores, therefore the degree of crystallinity relative to the relevant physical mixture yields an estimate of the degree of confinement of LiH. Several samples were repeated to deduce the error of the measurement which was found to be 6% of the degree of crystallinity, for example the error of a sample with 52% crystallinity would be ±3%. The crystallite sizes were determined from the peak width of the LiH XRD peaks according to the Scherrer method, ensuring that a minimum of 5 data points were present above the full width half maximum [33].

Nitrogen physisorption: measurements were performed at 77 K using a Micromeritics TriStar instrument. Micropore volumes (<1 nm) were calculated using the t-plot method and mesopore volumes (between 1 and 300 nm) were determined using the adsorption branch of the Barrett–Joyner–Halenda (BJH) method. The BJH pore size distributions of the support and nanocomposites were determined using the adsorption branch of the isotherm with carbon black as a reference. The volume average pore diameter was taken as the peak (average value) of the resulting profile. The particle size distribution of the LiH in the nanocomposites was estimated by subtracting the pore size distribution of the nanocomposite from that of the corresponding leached sample. In this way the volume of the pores occupied by LiH was estimated and could be assumed to correspond to the particle sizes of the LiH particles contained within the pore structure. The average value of this particle size distribution was used as the average particle size of LiH in each nanocomposite. These data are summarized in Table 2.

Scanning electron microscopy (SEM): was performed using an FEI XL30 FEG SEM instrument in secondary electron mode at an acceleration voltage of 15 kV. Samples were passivated in air and sputter-coated with 8 nm of Pt before loading into the SEM instrument. The LiH particles were identified by comparison of images of the nanocomposites to the images of the

Table 2 – Summary of nitrogen physisorption data for the supports and nanocomposites prepared.

Entry	BET surface area/$m^2\ g^{-1}$	Micropore volume/$cm^3\ g^{-1}$	Micropore volume loss/$cm^3\ g^{-1}$	Mesopore volume/$cm^3\ g^{-1}$	Pore size range/nm[b]
CX18	604	0.17		0.64	2–35 (18)
HSAG	578	0.08		0.69	2–100 (2)
CX18_n_300	186	0.01	0.16[a]	0.45	2–35 (19)
CX18_n_100	214	0.02	0.15[a]	0.53	5–35 (21)
CX18_t_300	196	0.00	0.17[a]	0.63	2–35 (22)
CX18_t_100	169	0.01	0.16[a]	0.32	2–35 (9)
HSAG_n_300	220	0.02	0.06[a]	0.37	2–100 (2)
HSAG_t_100	249	0.00	0.08[a]	0.33	2–100 (2)

[a] Indicates pore blocking.
[b] The number in brackets represents the average pore diameter.

supports obtained under the same conditions. The particle size distribution of the LiH particles on the surface of the support was measured by determining the particle size of at least 300 particles for each nanocomposite and the average size of these particles is given as the particle size. Particle sizes could not be measured in this manner for the HSAG-supported nanocomposites as it was not possible to reliably distinguish between the support and the LiH particles (see Supporting information Fig. S2.3).

Temperature programmed desorption (TPD): measurements were performed by loading roughly 50 mg of sample into a Micromeritics AutoChem II (Ar flow of 25 $cm^3\ min^{-1}$, temperature ramp of 5 °C min^{-1}), equipped with a TCD detector in order to monitor the decomposition of LiH. In order to ensure the samples were not exposed to air before measurement they were prepared in the glovebox by adding the measured amount of sample to the quartz reactor and using rubber stoppers on both openings of the reactor. The reactor was then removed from the glovebox and promptly taken to the TPD instrument where the reactor was connected under 50 mL min^{-1} Ar flow to ensure no contact between air and the sample. The measured error in quantification of the hydrogen released is 0.2–0.3 wt%. To check whether all butyllithium had decomposed and all solvent removed, mass spectrometric analysis was performed using a Pfeiffer Omnistar mass analyzer coupled to the Micromeritics TPD apparatus during measurement. This was done by monitoring the m/z peaks corresponding to the 1-butene released during decomposition of butyllithium (m/z = 41) as well as the hexane (m/z = 57) or pentane (m/z = 43) solvent during heating in the TPD instrument. As a means of comparison of TPD-MS results for the nanocomposites the TPD-MS profile of a mixture of t-butyllithium solution and the carbon xerogel support was measured. For this roughly 100 mg of the carbon support was mixed with 1 cm^3 of 1-butyllithium solution and 50 mg of this mixture was used in the TPD-MS measurement.

Reversibility studies: Hydrogen absorption was measured using a Sievert-type apparatus (PCT Pro-2000, Hy-Energy & Setaram, pressure measurement accuracy: 1% of reading) using roughly 100 mg of nanocomposite. Prior to absorption the hydrogen was desorbed from the sample at 350 °C for 30 min under 50 $cm^3\ min^{-1}$ of Ar flow before loading into the Sievert Instrument. Hydrogen absorption was performed by pressurizing the sample with hydrogen at 200 °C and measuring the kinetics of absorption by monitoring the pressure decrease over time. This was performed for pressures from 1 to 50 bar in increments of increasing in size logarithmically starting from 0.1 bar steps where the next aliquot of hydrogen was added once equilibrium had been reached (where no more changes in pressure were observed). The total molar quantity of hydrogen absorbed was calculated as a gravimetric quantity from the recorded pressure drop at each pressure increment. Following hydrogen uptake measurements XRD and TPD measurements of the sample were performed to ensure that this hydrogen uptake was reversible (Supporting information Figs. S3.1–S3.3).

Results and discussion

Structural characterization of the LiH/C nanocomposites

The nanocomposites were prepared using the method outlined in Scheme 1. Characterization of the LiH particles is a major challenge as they cannot be imaged by commonly used techniques such as transmission electron microscopy. For this reason a number of complimentary techniques that yield information on the LiH/C nanocomposite have been utilized. Specific properties of interest include: the amount of butyllithium (BuLi) precursor and the solvent it was dissolved in remaining in the sample, the amount of LiH, the particle size and the quantification of the amount of LiH inside and outside of the support pore system. In the following section the CX18_n_300 nanocomposite will be used as an example to illustrate how each of these parameters were measured.

Temperature programmed desorption coupled to mass spectrometry (TPD-MS) was used to examine both the extent of butyllithium decomposition as well as the success of the drying step (Supporting information Fig. S4.1). Only 2% of the 1-butene or solvent remained in the sample so it can be concluded that the procedure allows the preparation of LiH particles with minimal contamination of any of the components of the precursor solution.

The second parameter was the amount and crystallite size of crystalline LiH, which were determined using XRD. Fig. 1 shows the X-ray diffractogram of the CX18_n_300 sample. The presence of crystalline LiH is clear, represented by the reflections at 44.5° (111), 51.9° (200) and 77.0° (220). In XRD the LiH peaks are sharp and intense for both CX18_n_300 and CX18_n_300_PM, which have crystallites greater that 30 nm in

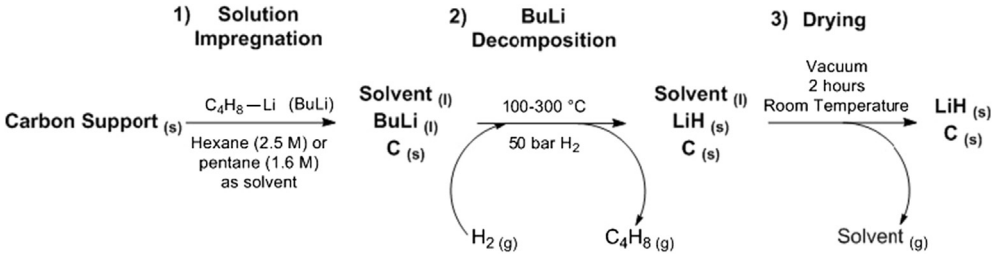

Scheme 1 – Overview of the procedure for preparing carbon supported LiH by solution impregnation of butyllithium (BuLi).

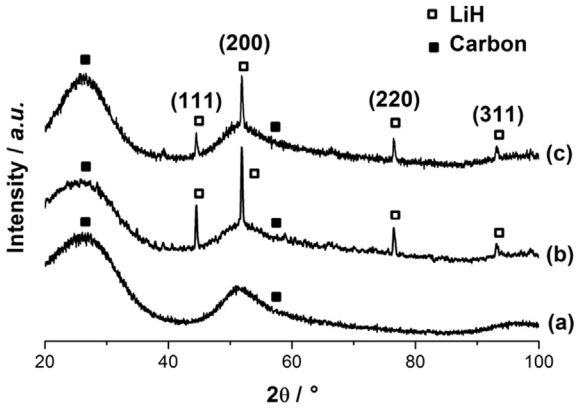

Fig. 1 – X-ray diffraction pattern of (a) carbon xerogel with volume average pore diameter of 18 nm (CX18), (b) CX18_n_300_PM physical mixture and (c) CX18_n_300. XRD patterns are normalized to the main carbon peak at around 30° in each sample and offset for clarity.

size. The crystallite size can be indicative of the particle size but particles lacking long range crystallinity are not visible in XRD.

The lower fraction of crystalline LiH in CX18_n_300 compared to CX18_n_300_PM indicates that a large fraction of the particles are either too small or too amorphous to detect. The sample contains two populations of LiH: the crystalline population which is observed in XRD and the population that is not observed by XRD as it lacks long range crystallinity. CX18_n_300 contains only 52% crystalline LiH compared to the CX18_n_300_PM physical mixture. In general it can be assumed that confinement in the pores leads to relatively small particles hence the degree of confinement also indicates the number of smaller particles present.

Fig. 2 shows the pore size distribution, obtained from nitrogen physisorption, of the carbon support and the CX18_n_300 nanocomposite. The pore size distribution of the nanocomposite is broad, with an average at 19 nm, which is very similar to the pore size distribution of the support, suggesting that the pore structure influences the LiH particle size distribution. When comparing the pore size distribution of the support to the nanocomposite the missing pore volume can be assumed to be occupied by LiH. The particle size distribution of the LiH particles confined to the pores can therefore be inferred by subtracting the pore size distribution of the nanocomposite from the leached nanocomposite (where all LiH has been removed). The resulting distribution of pore volume loss shown in Fig. 2 represents the LiH particle size distribution which has a continuous range of particle sizes from 2 to 35 nm. Further, there is a loss of 90% of the micropore volume, which suggests a significant proportion of particles smaller than 2 nm, or alternatively this may be due to micropore blocking. The reduction in mesopore volume of 0.18 $cm^3 g^{-1}$ corresponds to 87% of the volume of the LiH in the nanocomposite, showing that at least 13% is on the outer surface. This does corroborate the degree of confinement (48%) determined from the crystallinity of LiH in the nanocomposite. This difference can be explained as blocking of some of the carbon porosity, and/or some of the crystals residing in the relatively large pores contributing to the XRD signal. In principle the physisorption gives the higher estimate (87%) of pore confinement while the XRD gives the lower limit (48%).

The pore size distribution of HSAG_n_300 is also shown in Fig. 2, which highlights the differences between the two supports. CX18 has a very different pore size distribution to HSAG where the majority of pores are around 2 nm with a continuous distribution up to around 100 nm. The majority of the pores in HSAG are also significantly smaller than in CX18 as much of the pores in HSAG are less than 10 nm in diameter. The LiH particle size distribution follows the pore size distribution of the support: in HSAG_n_300 most particles are smaller than 10 nm with a peak at around 2 nm.

For the CX18_n_300 nanocomposite the particles on the outside of the carbon support can be directly observed through SEM. This means that the particle size for the large LiH particles on the external surface of the support can be estimated. Fig. 3 shows the SEM images of CX18_n_300 and the bare CX18 support. Clear observation of the LiH particles is possible as the mostly featureless faces of the carbon xerogel support allow a strong contrast between LiH and support. The particles vary in size from below 1 μm–10 μm with most in the range of 1–6 μm.

The particle size has been shown to influence the temperature of hydrogen release from metal hydrides [13,34]. This means that measuring the H_2 release profile is another way of estimating particle size ranges and can be compared to XRD, nitrogen physisorption and SEM to illustrate the different LiH particle sizes present. Fig. 4 shows the hydrogen release profile of CX18_n_300 as well as that of LiH and the CX18_n_300_PM physical mixture. The onset of hydrogen release occurs at 170 °C in the nanocomposite while the macrocrystalline system has an onset of 450 °C, a difference of 280 °C. This result can be assumed to be due to the smaller LiH particle size and confinement within the pore system [27]. The

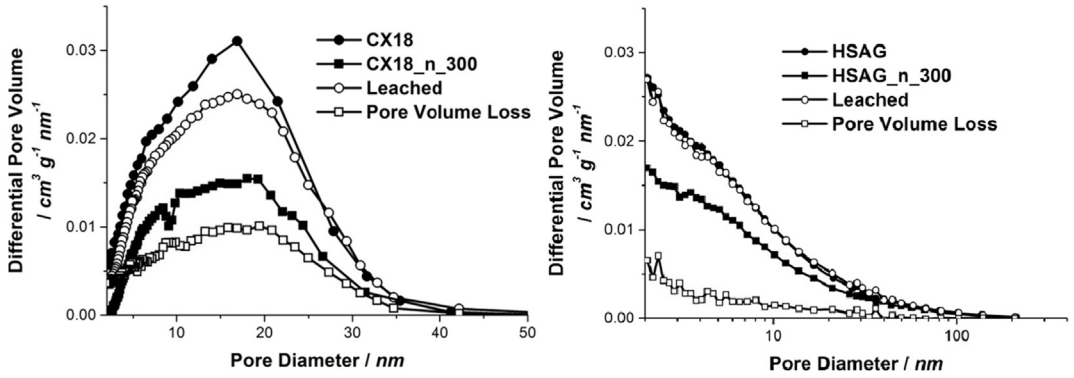

Fig. 2 – Left: Pore size distributions obtained from nitrogen physisorption for CX18, CX18_n_300 and CX18_n_300 following leaching. Right: Pore size distributions obtained from nitrogen physisorption for HSAG, HSAG_n_300 and HSAG_n_300 following leaching. The pore volume loss distribution is calculated by subtracting the impregnated distribution from the leached distribution.

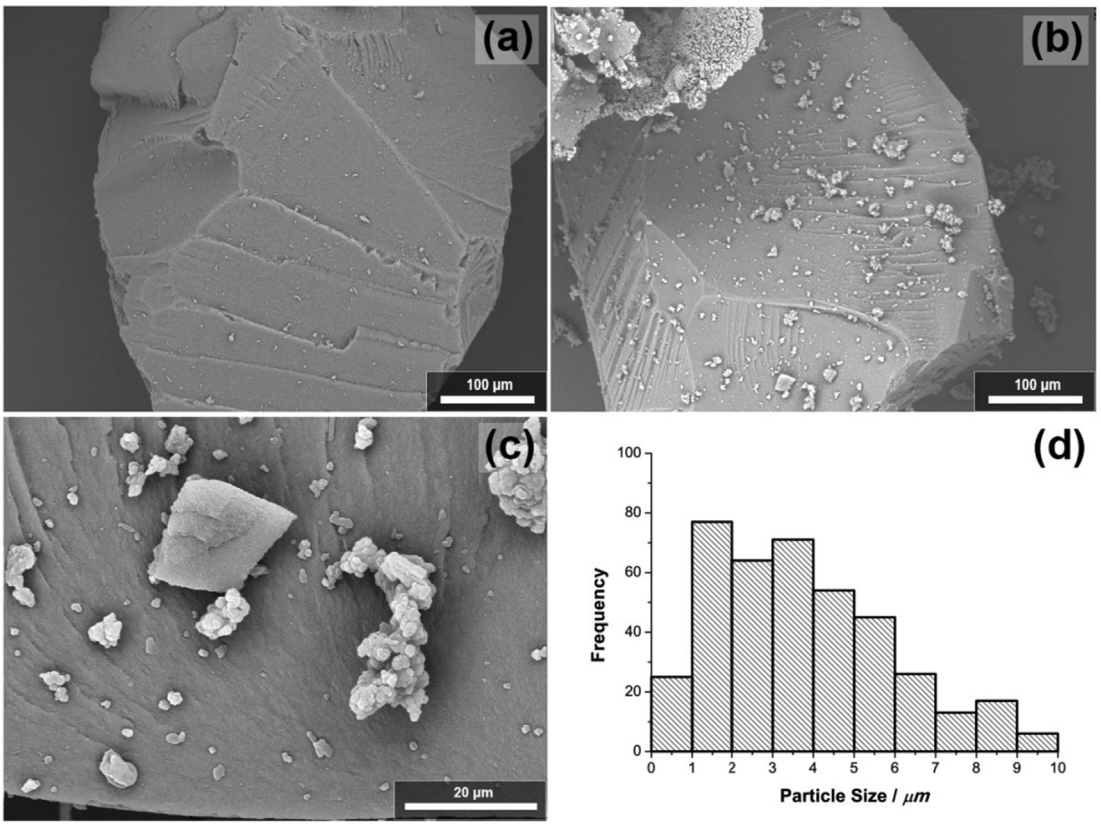

Fig. 3 – Scanning electron microscopy (SEM) images of (a) CX18, (b and c) CX18_n_300 and (d) a histogram representing the distribution of particle sizes observed through SEM.

total amount of hydrogen released amounts to 10.9 wt% w.r.t. LiH (1.7 wt% w.r.t. the sample), while the theoretical maximum is 12.6 wt%.

The hydrogen release profile of CX18_n_300 can be divided into two main regions. The hydrogen release in the range 400–600 °C can be attributed to non-confined LiH on the external surface of the support, which is similar to the CX18_n_300_PM physical mixture. Therefore any release beginning below 400 °C is likely from confined LiH. The hydrogen release in the lower temperature region accounts for 85% of the total hydrogen release, which was determined by fitting the profile to 5 separate peaks and determining their contributions to the total hydrogen release (Fig. 4, right). This value is closer to the estimation of the confined fraction by physisorption than that by XRD which suggests that the pores also contain some crystalline LiH.

It is not clear why the confined LiH displays a release peak with several shoulders. It is possible that the shoulder

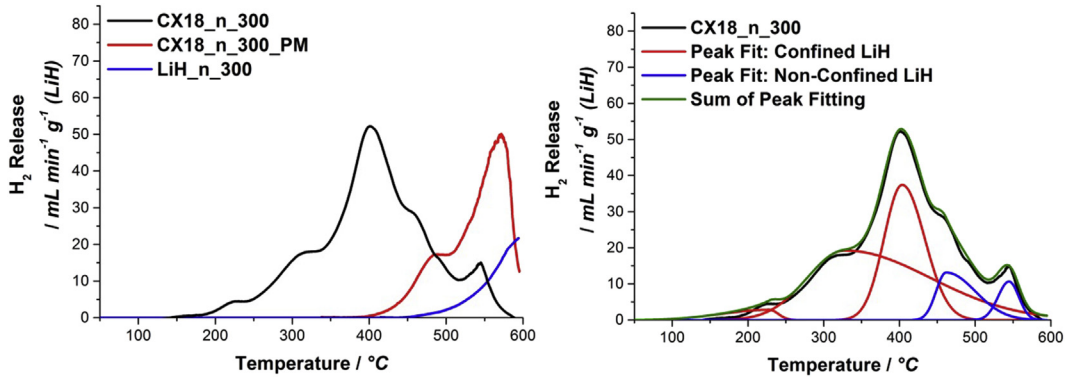

Fig. 4 – Left: Hydrogen release profile of CX18_n_300, the CX18_n_300_PM physical mixture and macrocrystalline LiH prepared by decomposing n-butyllithium at 300 °C under 50 bar hydrogen pressure. Right: Peak fitting of the hydrogen release profile of CX18_n_300. Measurements performed under a flow of 25 cm^3 min^{-1} Ar and temperature ramp of 5 °C min^{-1}.

occurring at the lowest temperature results from micropore confined LiH. An explanation for the remaining two pore-confined peaks is the presence of crystalline and non-crystalline LiH within the pores, where the non-crystalline LiH releases hydrogen at lower temperatures. This is supported by the XRD data which suggests 62% of the pore-confined LiH is non-crystalline and the second peak (peak temperature of roughly 300 °C) contributes 61% of the hydrogen release originating from pore-confined LiH. In addition the total amount of hydrogen released is significantly higher in CX18_n_300 at 10.9 wt% compared to its corresponding physical mixture (6.6 wt%), further demonstrating the influence of confinement and reduction of the particle size on the hydrogen release.

Studying effect of the preparation parameters

Although this procedure yields LiH particles supported on carbon, the fraction of confined LiH could still be improved. It is relevant to optimize the procedure to allow a greater degree of confinement and reduction of the fraction of crystalline LiH in order to further reduce the hydrogen release temperature. In addition, an understanding of the procedure used to prepare these particles would be beneficial for the preparation of other similar compounds. With this in mind several experimental parameters were varied and Table 3 shows a summary of the results. Each parameter will be discussed in detail in the following sections.

Effect of butyllithium precursor type and decomposition temperature

In the preparation of MgH_2 via dibutylmagnesium a temperature of 300 °C is used [30], however lower temperatures may promote the formation of smaller particles or crystallites. In addition to this, butyllithium occurs in several forms: n-butyllithium (n-BuLi) which exists as a hexamer in solution, whereas t-butyllithium (t-BuLi) exists as a tetramer [35]. For this reason the use of t-BuLi instead of n-BuLi may provide an additional reduction in LiH particle size or a higher proportion of confined LiH. With this in mind a series of nanocomposites were prepared using different decomposition temperatures and precursors.

The XRD data indicate that the decomposition temperature and precursor indeed have a large impact on the final LiH crystallite size, yielding 15 nm crystallites in CX18_t_100, compared to CX18_n_300 which has crystallites above 30 nm in size. The degree of crystallinity shows a decrease from 52% to 29% which suggests a larger fraction of non-crystalline LiH confined in the pores. The LiH particles outside of the pores are substantially smaller with an average of 1.5 μm compared to 4.8 μm in CX18_n_300. The fact that the crystallite and particle sizes observed in CX18_t_300 are significantly larger compared to CX18_t_100 shows that the temperature at which the precursor is reacted with hydrogen is the more important factor in control of the crystallite sizes.

The effect on the hydrogen release is also clear as the average temperature of hydrogen release generally decreases whenever t-BuLi is used or reaction is performed at lower temperatures (Fig. 5). The proportion of hydrogen released from pore-confined LiH increases from 85% in CX18_n_300 to 100% in CX18_t_100. In CX18_t_100 no peaks corresponding to non-confined LiH are observed, although there are a number of small shoulders on the main peak at higher temperatures that are likely due to small amounts of LiH on the external surface of the support. Further, the onset of hydrogen release in CX18_t_100 is 100 °C compared to 300 °C in the CX18_t_100_PM physical mixture. The synthesis parameters are clearly very important in determining the outcome of the synthesis and the resulting hydrogen release profile, but further control of the particle size may be achieved by changing the nature of the support.

Effect of support type

The pore characteristics and surface properties of different forms of carbon can have an influence on the particle size and the decomposition profile [20,36]. Carbon xerogels are amorphous supports with a broad distribution of mesopores. It would be of interest to also test a support that is more graphitic in nature with smaller pores in order to investigate the impact that interaction between LiH and the support as well as the pore structure have on the hydrogen sorption

Table 3 – Influence of conditions of butyllithium decomposition on final LiH crystallite, crystallinity and particle size. The degree of crystallinity and crystallites size was determined from X-ray diffraction, mesopore volume loss from nitrogen physisorption and external particle size was determined from SEM.

Sample	Degree of LiH confinement			LiH Size		H_2 release w.r.t. LiH/wt%		
	Degree of crystallinity/%	Mesopore volume loss/$cm^3\ g^{-1}$	% LiH in Pores[a]	Crystallite size/nm	External particle size/μm	Confined LiH	Non-confined LiH	Total
CX18_n_300	52 ± 3	0.18	87	>30	4.8	9.3	1.6	10.9
CX18_n_300_PM	100			>30	30	0.0	6.6	6.6
CX18_n_100	35 ± 2	0.11	53	26	3.3	4.3	4.2	8.5
CX18_n_100_PM	100			17	22	0.0	8.7	8.7
CX18_t_300	57 ± 4	0.00	3	>30	3.2	5.7	2.5	8.2
CX18_t_300_PM	100			>30	28	0.0	4.3	4.3
CX18_t_100	29 ± 2	0.31	204[b]	11	1.5	10.4	0.0	10.4
CX18_t_100_PM	100			32	15	0.0	5.2	5.2
HSAG_n_300	100	0.32	151[b]	15		12.5	0.0	12.5
HSAG_n_300_PM	100			>30		0.0	12.2	12.2
HSAG_t_100	39 ± 3	0.36	233[b]	15		12.5	0.0	12.5
HSAG_t_100_PM	100			26		0.0	9.9	9.9

[a] Calculated from mesopore volume loss. Given as a percentage of the LiH contained within the sample.
[b] Indicates pore blocking.

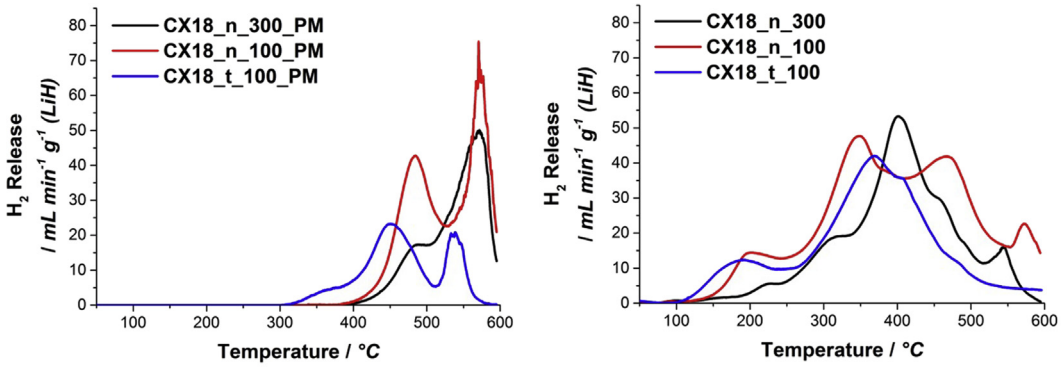

Fig. 5 – Comparison of the effect of temperature of butyllithium decomposition (300 °C and 100 °C) and butyllithium precursor (n-butyllithium and t-butyllithium) on the hydrogen release profile. Left: LiH/CX18 physical mixtures, right: LiH/CX18 nanocomposites. TPD measurements performed under a flow of 25 $cm^3\ min^{-1}$ Ar and temperature ramp of 5 °C min^{-1}.

characteristics. For this reason high surface area graphite (HSAG, surface area 578 $m^2\ g^{-1}$) was tested as a support for the LiH particles in addition to the carbon xerogel support discussed in the previous sections.

In evaluating the differences between the CX18 and HSAG-supported nanocomposites the particle size and degree of confinement should be considered. The particle size range according to nitrogen physisorption is similar to CX18_n_300 but with a higher proportion of particles less than 10 nm in size. It is important to note that the LiH particles cannot be observed using SEM in the HSAG-supported examples as it is not possible to distinguish between the support and the LiH particles (Supporting information Fig. S2.3). The degree of confinement, determined from the degree of crystallinity, in HSAG_t_100 is 39%, which is higher than 29% in CX18_t_100.

A very striking difference between HSAG and CX18 is that even the physical mixture (HSAG_t_100_PM) has a very low hydrogen release temperature compared to the macrocrystalline system (Fig. 6). HSAG_t_100_PM begins release at 200 °C while CX18_t_100_PM begins release at 300 °C. The physical mixture hydrogen release profile also resembles a LiH/HSAG nanocomposite reported in the literature, where the HSAG_t_100 nanocomposite displays hydrogen release at temperatures roughly 100 °C lower [24]. The difference between HSAG and CX18 may be due to a better contact between LiH and carbon in HSAG_t_100_PM compared to CX18_t_100_PM [37,38] or the stronger electronic effects in the more graphite-like HSAG, while CX18 is an amorphous carbon material. Alternatively, formation of Li_2O by reaction between LiH and surface oxygen sites on the support may provide an explanation as HSAG has a higher density of surface oxygen sites compared to CX18. In addition, HSAG_t_100 releases 12.5 wt% of hydrogen (close to the theoretical maximum), while CX18_t_100 releases 10.4 wt%. The onsets of 100 °C in CX18_t_100 and HSAG_t_100 are also significantly lower than the 200 °C reported previously in the literature [27]. Such a striking improvement on the hydrogen release properties of LiH could have important implications

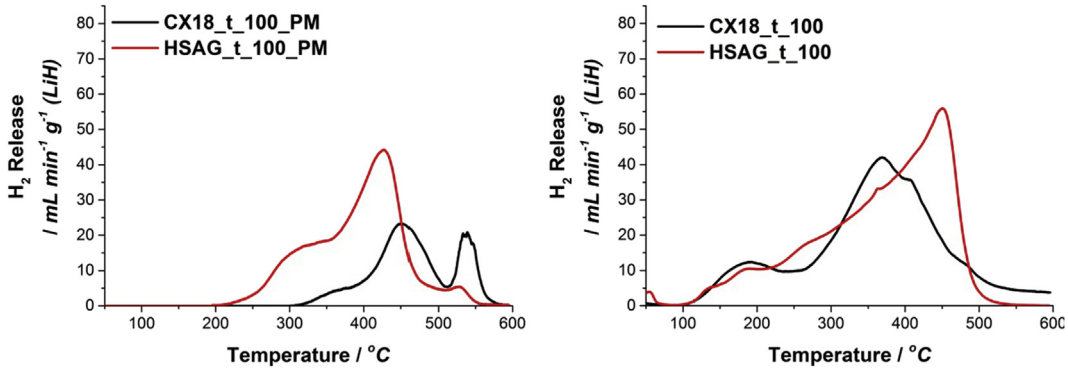

Fig. 6 – Temperature programmed desorption profiles of samples prepared on high surface area graphite (HSAG_t_100), and carbon xerogel (CX18_t_100) compared to their corresponding LiH/C physical mixtures (HSAG_t_100_PM and CX18_t_100_PM respectively). TPD measurements performed under a flow of 25 cm^3 min^{-1} Ar and temperature ramp of 5 °C min^{-1}.

for the development of solid state hydrogen storage materials, but the important question is whether or not this hydrogen release is reversible.

Reversibility of hydrogen desorption

Fig. 7 shows the hydrogen uptake of the HSAG and CX18-supported nanocomposites following desorption at 350 °C. The equilibrium uptake pressure is low as hydrogen uptake begins at pressures as low as 0.1 bar, where much of the total capacity is absorbed. The quantity of hydrogen absorbed in dehydrogenated CX18_t_100 is 7.0 wt%, while HSAG_t_100 and CX18_n_300 absorb 2.3 wt% and 0.4 wt% respectively. In CX18_n_300 only roughly 0.1 wt% of hydrogen is absorbed below 1 bar, unlike the other two samples which demonstrate hydrogen uptake of 1.5–5 wt% below 1 bar, which is the majority of their total uptake. This is likely due to the fact that CX18_n_300 has a lower degree of confined LiH compared to CX18_t_100 and HSAG_t_100, as evidenced in the previous sections. As a result CX18_n_300 releases less hydrogen below 350 °C than the other samples which limits its reversible capacity. The difference in hydrogen uptake between HSAG_t_100 and CX18_t_100 is also quite striking as HSAG_t_100 absorbs 4.7 wt% less hydrogen than CX18_t_100. This may be due to formation of Li_2O from reaction between LiH and the higher density of surface oxygen sites present in HSAG compared to CX18.

Temperature programmed desorption measurements (Supporting information Fig. S3.3) following rehydrogenation of these nanocomposites demonstrate that this uptake is also reversible with 6–7 wt% of hydrogen released. This illustrates how optimization of the preparation procedure and support improves the hydrogen sorption characteristics as seen in the previous sections. However, it is not yet clear why HSAG_t_100 releases more hydrogen yet a smaller portion of this is reversible compared to CX18_t_100.

The kinetics of hydrogen absorption are rapid for all three nanocomposites where 80% of the total hydrogen capacity is absorbed within 15 s under a pressure of 26 bar at 200 °C. Such rapid hydrogen uptake can be explained by the high affinity metallic lithium has for hydrogen. Li metal is also liquid at 200 °C which affords increased mobility. The kinetics in CX18_t_100 and CX18_n_300 are very similar while the HSAG_t_100 displays significantly faster kinetics than the others. This may be a result of the better contact between the carbon and Li catalyzing the hydrogen uptake or the larger

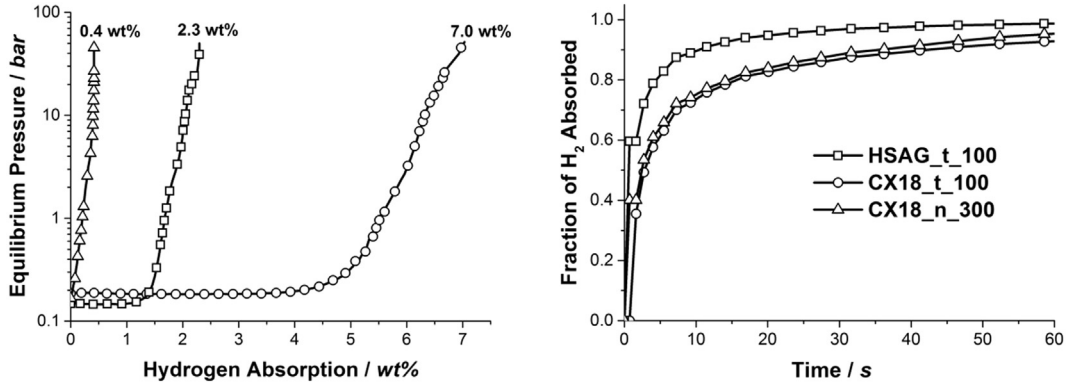

Fig. 7 – Left: Hydrogen uptake as a function of hydrogen pressure of HSAG_t_100, CX18_t_100 and CX18_n_300 measured at 200 °C. Right: Rate of hydrogen absorption at 200 °C, 26 bar. Hydrogen desorption from each sample was performed at 350 °C for 30 min before measurement.

proportion of small Li particles yielding a higher fraction of liquid Li. The ability of this nanocomposite to not only reversibly store hydrogen, while the uptake occurs at low pressures, is a very promising result for the field of hydrogen storage as this has not been demonstrated in the literature with such high loadings of LiH [27].

Conclusions

Carbon supported LiH nanoparticles have been successfully prepared which, to the best of our knowledge, has previously not been reported. The procedure consists of solution impregnation of a porous carbon materials with butyllithium and subsequent decomposition under hydrogen yields LiH nanoparticles. It was determined that confinement of the LiH facilitates release of hydrogen at lower temperatures and therefore the effect of a number of parameters on the degree of confinement has been examined:

- Reaction parameters: reducing this temperature from 300 °C to 100 °C and using a t-butyllithium precursor instead of an n-butyllithium precursor yields a higher degree of confinement (85% when 300 °C, n-butyllithium is used and 100% when 100 °C, t-butyllithium is used).
- Support type: better contact between the high surface area graphite support and LiH allows higher gravimetric hydrogen release (12.5 wt%) but lower levels of hydrogen uptake (2.3 wt%, compared to 7.0 wt% in the carbon xerogel supported case).

The conditions with which the highest degree of confinement and highest reversible hydrogen capacity are obtained are: carbon xerogel type support, using a t-butyllithium precursor and decomposing it at 100 °C.

The nanocomposite demonstrates strongly reduced LiH decomposition temperatures compared to the macrocrystalline and physical mixture systems due to confinement effects. The optimized preparation of the LiH/C gives a nanocomposite that begins hydrogen release as low as 100 °C and 10.4 wt% (of LiH) is released. Uptake of up to 7.0 wt% can be performed at 200 °C and as low as 0.1 bar H_2 pressure, while full uptake can occur within 5 min at 26 bar, which has so far not been achieved through any other method of LiH modification. In short a procedure for preparing a novel nanocomposite has been developed and a variety of conditions can be used to tune the degree of LiH confinement and reversible hydrogen capacity.

Acknowledgements

The authors would like to acknowledge Krijn de Jong for useful scientific discussions as well as Rien van Zwienen, Jan-Willem de Rijk and Marjan Versluis-Helder for technical support. The authors would also like to thank the Netherlands Organization for Scientific Research (NWO-ECHO, grant number 712.012 .004) for funding the project.

Appendix A. Supplementary data

Supplementary data related to this article can be found at http://dx.doi.org/10.1016/j.ijhydene.2016.10.062.

REFERENCES

[1] Chen P, Xiong Z, Luo J, Lin J, Tan KL. Interaction of hydrogen with metal nitrides and imides. Nature 2002;420:302–4.
[2] Jepsen J, Bellosta von Colbe JM, Klassen T, Dornheim M. Economic potential of complex hydrides compared to conventional hydrogen storage systems. Int J Hydrogen Energy 2012;37:4204–14.
[3] Gislon P, Prosini PP. Devices for producing hydrogen via $NaBH_4$ and LiH hydrolysis. Int J Hydrogen Energy 2011;36:240–6.
[4] Unemoto A, Matsuo M, Orimo S. Complex hydrides for electrochemical energy storage. Adv Funct Mater 2014;24:2267–79.
[5] Dong BX, Chen LT, Teng YL, Gao JJ, Tian H. Effect of alkali metal amides on the improvement of dehydrogenation for the LiH-NH_3 system. J Mater Sci 2016;51:911–6.
[6] Abbas MA, Grant DM, Brunelli M, Hansen TC, Walker GS. Reducing the dehydrogenation temperature of lithium hydride through alloying with germanium. Phys Chem Chem Phys 2013;15:12139.
[7] Jain A, Kawasako E, Miyaoka H, Ma T, Isobe S, Ichikawa T, et al. Destabilization of LiH by Li insertion into Ge. J Phys Chem C 2013;117:5650–7.
[8] Jia Y, Sun C, Shen S, Zou J, Mao SS, Yao X. Combination of nanosizing and interfacial effect: future perspective for designing Mg-based nanomaterials for hydrogen storage. Renew Sustain Energy Rev 2015;44:289–303.
[9] Reshak AH. MgH_2 and LiH metal hydrides crystals as novel hydrogen storage material: electronic structure and optical properties. Int J Hydrogen Energy 2013;38:11946–54.
[10] Zhou S, Zhang X, Li T, Wang N, Chen H, Zhang T, et al. Nano-confined magnesium for hydrogen storage from reactive milling with anthracite carbon as milling aid. Int J Hydrogen Energy 2014;39:13628–33.
[11] Sartbaeva A, Wells SA, Sommariva M, Lodge MJT, Jones MO, Ramirez-Cuesta AJ, et al. Formation of crystalline sodium hydride nanoparticles encapsulated within an amorphous framework. J Clust Sci 2010;21:543–9.
[12] Leng H, Pan Y, Li Q, Chou KC. Effect of LiH on hydrogen storage property of MgH_2. Int J Hydrogen Energy 2014;39:13622–7.
[13] Miyaoka H, Tange K, Yamamoto H, Hino S, Ichikawa T, Kojima Y. Correlation between particle size and hydrogen generation properties on ammonia and lithium hydride system. Int J Hydrogen Energy 2015;40:14911–5.
[14] Haertling C, Hanrahan RJ, Smith R. A literature review of reactions and kinetics of lithium hydride hydrolysis. J Nucl Mater 2006;349:195–233.
[15] Varin RA, Jang M. The effects of graphite on the reversible hydrogen storage of nanostructured lithium amide and lithium hydride ($LiNH_2$ + 1.2LiH) system. J Alloys Compd 2011;509:7143–51.
[16] Ngene P, Verkuijlen MHW, Barre C, Kentgens APM, de Jongh PE. Reversible Li-insertion in nanoscaffolds: a promising strategy to alter the hydrogen sorption properties of Li-based complex hydrides. Nano Energy 2016;22:169–78.
[17] Friščić T, Halasz I, Beldon PJ, Belenguer AM, Adams F, Kimber SAJ, et al. Real-time and in situ monitoring of mechanochemical milling reactions. Nat Chem 2013;5:66–73.

[18] Léon A, Zabara O, Sartori S, Eigen N, Dornheim M, Klassen T, et al. Investigation of (Mg, Al, Li, H)-based hydride and alanate mixtures produced by reactive ball milling. J Alloys Compd 2009;476:425–8.
[19] de Jongh PE, Wagemans RWP, Eggenhuisen TM, Dauvillier BS, Radstake PB, Meeldijk JD, et al. The preparation of carbon-supported magnesium nanoparticles using melt infiltration. Chem Mater 2007;19:6052–7.
[20] Au YS, Obbink MK, Srinivasan S, Magusin PCMM, De Jong KP, De Jongh PE. The size dependence of hydrogen mobility and sorption kinetics for carbon-supported MgH_2 particles. Adv Funct Mater 2014;24:3604–11.
[21] Adelhelm P, Gao J, Verkuijlen MHW, Rongeat C, Herrich M, van Bentum PJM, et al. Comprehensive study of melt infiltration for the synthesis of $NaAlH_4$/C nanocomposites. Chem Mater 2010;22:2233–8.
[22] Yoshida A, Mori Y, Watanabe M, Naito S. Hydrogen storage materials comprising conjugated hydrocarbon polymers with LiH: comparison of cyclic durability between LiH–Polyacetylene, –Poly(p-phenylene), and –Poly(diphenylacetylene) and mechanistic investigation upon LiH–Poly(p-phenylene). J Phys Chem C 2014;118:19683–7.
[23] Stasch A. Well-defined, nanometer-sized LiH cluster compounds stabilized by pyrazolate ligands. Angew Chem Int Ed 2014;53:1338–41.
[24] Wang L, Quadir MZ, Aguey-Zinsou K-F. Direct and reversible hydrogen storage of lithium hydride (LiH) nanoconfined in high surface area graphite. Int J Hydrogen Energy 2016;41:18088–94.
[25] Dujardin E, Ebbesen TW, Hiura H, Tanigaki K. Capillarity and wetting of carbon nanotubes. Science 1994;265:1850–2.
[26] Dujardin E, Ebbesen TW, Krishnan A, Treacy MMJ. Wetting of single shell carbon nanotubes. Adv Mater 1998;10:1472–5.
[27] Huang L, Bonnet J-P, Zlotea C, Bourgon J, Latroche M, Courty M, et al. Synthesis of destabilized nanostructured lithium hydride via hydrogenation of lithium electrochemically inserted into graphite. Int J Hydrogen Energy 2015;40:13936–41.
[28] Munnik P, de Jongh PE, de Jong KP. Recent developments in the synthesis of supported catalysts. Chem Rev 2015;115:6687.
[29] Stasch A. A hydrocarbon-soluble lithium hydride complex. Angew Chem Int Ed 2012;51:1930–3.
[30] Zhang S, Gross AF, Van Atta SL, Lopez M, Liu P, Ahn CC, et al. The synthesis and hydrogen storage properties of a MgH_2 incorporated carbon aerogel scaffold. Nanotechnology 2009;20:204027.
[31] Nielsen TK, Manickam K, Hirscher M, Besenbacher F, Jensen TR. Confinement of MgH_2 nanoclusters within nanoporous aerogel scaffold materials. ACS Nano 2009;3:3521–8.
[32] Al-Muhtaseb SA, Ritter JA. Preparation and properties of resorcinol-formaldehyde organic and carbon gels. Adv Mater 2003;15:101–14.
[33] Langford JI, Wilson AJC. Scherrer after sixty years: a survey and some new results in the determination of crystallite size. J Appl Crystallogr 1978;11:102–13.
[34] Friedrichs O, Kolodziejczyk L, Sánchez-López JC, Fernández A, Lyubenova L, Zander D, et al. Influence of particle size on electrochemical and gas-phase hydrogen storage in nanocrystalline Mg. J Alloys Compd 2008;463:539–45.
[35] Elschenbroich C. Organometallics, Wiley. 2006.
[36] Gao J, Adelhelm P, Verkuijlen MHW, Rongeat C, Herrich M, van Bentum PJM, et al. Confinement of $NaAlH_4$ in nanoporous carbon: impact on H2 release, reversibility, and thermodynamics. J Phys Chem C 2010;114:4675–82.
[37] Adelhelm P, de Jongh PE. The impact of carbon materials on the hydrogen storage properties of light metal hydrides. J Mater Chem 2011;21:2417.
[38] Berseth PA, Harter AG, Zidan R, Blomqvist A, Araujo CM, Scheicher RH, et al. Carbon nanomaterials as catalysts for hydrogen uptake and release in $NaAlH_4$. Nano Lett 2009;9:1501.